## SUPPLEMENTAL INFORMATION

## EXTENDED EXPERIMENTAL PROCEDURES

**Clinical Protocol.** Nine patients with NSCLC were enrolled in an IRB-approved protocol after obtaining informed consent. On the day of surgery, a bolus of 8g over 10 minutes followed by 8g/hr continuous infusion of pyrogen-free [U-$^{13}$C]glucose from Cambridge Isotope Laboratories was administered through a peripheral intravenous line (PIV). A second PIV in the contralateral arm was used to obtain blood to analyze $^{13}$C enrichment in glucose. Standard surgical procedures were followed, with the majority of cases being robotic lobectomies. Based on pre-operative imaging and gross inspection at resection, viable fragments of tumor and lung were sampled. In cases where metabolic heterogeneity was assessed, the resected lobe was oriented anatomically to identify regions of the tumor pre-selected by imaging. Tissue fragments were washed in ice-cold saline and immediately frozen in liquid nitrogen so that the total time between resection and freezing averaged 4 to 5 minutes. All histological analyses were conducted by surgical pathologists blinded to the results of the metabolic study.

**Multi-parametric Magnetic Resonance Imaging (mpMRI).** MRIs occurred no more than 8 days before surgery on either a 3T dual-transmit Achieva MR scanner (Philips Healthcare, Best, The Netherlands) with a 16-channel SENSE-XL Torso Coil or a 3T Philips Ingenia scanner with a 28-channel dStream Anterior-Posterior coil (Philips Healthcare, Best, The Netherlands). Coronal and axial T2-weighted half-Fourier single-shot turbo spin-echo images were acquired for anatomic reference for localizing the lesion. Dynamic contrast enhanced (DCE) MRI was performed using a 2D or 3D T1-weighted spoiled gradient-echo sequence before, during, and after the administration of a bolus of 0.01 mmol/kg gadobutrol (Gadavist; Bayer Healthcare Pharmaceuticals) using a power injector at a rate of 2 cc/sec followed by a 20 cc saline flush at the same rate. DCE images were acquired with free-breathing for at least 4 minutes using the following parameters: TE/TR = 1.14-1.65/2.5-4.5 ms, flip angle = $10^{o}$, field of view = 200-300 x 200-300 mm$^2$, in-plane resolution = 0.8-1.7 x 0.8-1.7 mm$^2$, and temporal resolution = 0.5-5.2 sec. One or more imaging slices were acquired from the lesion with careful planning to avoid possible artifacts from the heart and major blood vessels.

Tumor volume measurements were based on T2-weighted images by ROI segmentation in an Open-Source DICOM Viewer, Osirix. DCE MRI was analyzed by manually drawn regions of interest (ROIs) in Osirix. For assessing regional DCE signal enhancement, ROIs of the same size were manually defined according to anatomical descriptors that could guide tissue procurement (e.g. prominent blood vessels or other landmarks). ROIs were then automatically propagated throughout the whole time series. Average ROI values were plotted at every available time point, and subtracted by the baseline signal, i.e., the ROI value immediately before contrast enhancement, which was assigned to time 0. Contrast enhancement curves were generated using Excel Solver to calculate constants of a gamma variate function that satisfy a minimum among all data points of a DCE scan and the points of a gamma variate function. Initial area under the curve measurements were approximated with the trapezoidal rule over the first 60 seconds post-contrast injection.

**Mass Spectrometry**. Blood was obtained prior to and approximately every 30 minutes during infusion of [U-$^{13}$C]glucose until tissue was removed from the patient. Whole blood was chilled on ice and centrifuged to separate and freeze the plasma. Aliquots of 50-100µl of plasma were added to 80:20 methanol:water for extraction. 50-100mg of frozen tissue fragments were added to 50:50 methanol:water and extracted to analyze $^{13}$C enrichment. Samples were subjected to three freeze-thaw cycles, then centrifuged at 16,000x*g* for 15 minutes to precipitate macromolecules. The supernatants, with 10µl of sodium oxybutyrate added as an internal control, were evaporated, derivatized in 150µl of a trimethylsilyl donor (TriSil, Pierce) or N-(*tert*-butyldimethylsilyl)-N-methyltrifluoroacetamide (MTBSTFA), and analyzed using either an Agilent 6890 or 7890 gas chromatograph coupled to an Agilent 5973N or 5975C Mass Selective Detector, respectively. The observed distributions of mass isotopologues were corrected for natural abundance; the 459 and 369 ions were used to monitor TMS-derivatized 3-PG and PEP, respectively, and other metabolites were monitored as described (Cheng et al., 2011). Relative metabolite abundances were estimated by normalizing a metabolite's ion current to the product of the total ion current for all detected metabolites and protein content of the corresponding fragment determined using the Pierce BCA Protein Assay kit.

**NMR Spectroscopy.** Sample preparation was previously described (Maher et al., 2012). NMR spectroscopy was performed on a Varian ANOVA 14.1 T spectrometer (Agilent, Santa Clara, CA) equipped with a 3-mm broadband probe with the "observe" coil tuned to $^{13}$C (150 MHz). Proton decoupling was performed using a standard WALTZ-

16 pulse sequence. Carbon spectra were acquired under the following conditions: pulse flip angle 45°, repetition time 1.5 s, spectral width 35 kHz, number of data points 104,986, and number of scans ~23,000–30,000, requiring 20–25 h. Free induction decays were zero filled to 131,072 points and apodized with exponential multiplication. Relevant peak areas were determined using ACDLabs NMR Processor (Advanced Chemistry Development).

**Modeling.** Simulations in tcaSIM used 3-PG M+3 fractional enrichment as the lactate input, which is modeled as interchangeable with pyruvate fractional enrichment. PDH and PC were simulated from 0 to 1 in increments of 0.05. A total of 55,566 simulations were performed for each data set. The simulated citrate M+0-M+1, glutamate M+0-M+5, and malate M+0-M+4 were compared to the experimental data. The absolute difference between each isotopologue's experimental and simulated data was summed for each simulation, yielding a total delta. Simulations were ranked by total delta, and the simulation with the lowest total delta value was used for PDH and PC relative flux values.

**Statistics.** Patient-matched tumor and non-cancerous lung samples, as well as intratumoral samples processed on the same day, were analyzed by a paired Student's t-test. Intertumoral analysis of contrast enhancement and relative fractional enrichments was analyzed by unpaired Student's t-tests. Correlation plots were analyzed for significance with Pearson's product-moment correlation coefficients of the trend lines. All data were considered significant if $p < 0.05$.

**RNA-sequencing.** Tumor samples were homogenized in TRIzol (Thermo Fisher) and total RNA was extracted using the RNeasy Mini Kit (Qiagen). Three μg of RNA was processed for library preparation using the Ovation human FFPE RNA-Seq library system (NuGEN). Sequencing was performed on the Illumina NextSeq500 platform. Raw reads were aligned to human genome assembly hg19 using TopHat (Kim et al., 2013). Transcripts were assembled and abundance was estimated using Cufflinks (Trapnell et al., 2010). The number of reads aligned to gene exons was converted to FPKM units (number of fragments per kilobase per million reads mapped) using Cuffnorm (Trapnell et al., 2010). A set of 2,756 human metabolic genes (Possemato et al., 2011) was used for GSEA to define differentially expressed pathways between samples with high or low DCE signal. RNA-seq data was deposited in the Gene Expression Omnibus database under GSE74484.

**References**

Cheng, T., Sudderth, J., Yang, C., Mullen, A.R., Jin, E.S., Matés, J.M., and DeBerardinis, R.J. (2011). Pyruvate carboxylase is required for glutamine-independent growth of tumor cells. Proceedings of the National Academy of Sciences *108*, 8674-8679.

Kim, D., Pertea, G., Trapnell, C., Pimentel, H., Kelley, R., and Salzberg, S.L. (2013). TopHat2: accurate alignment of transcriptomes in the presence of insertions, deletions and gene fusions. Genome biology *14*, R36.

Maher, E.A., Marin-Valencia, I., Bachoo, R.M., Mashimo, T., Raisanen, J., Hatanpaa, K.J., Jindal, A., Jeffrey, F.M., Choi, C., Madden, C., *et al.* (2012). Metabolism of [U-13C]glucose in human brain tumors in vivo. NMR in Biomedicine *25*, 1234-1244.

Possemato, R., Marks, K.M., Shaul, Y.D., Pacold, M.E., Kim, D., Birsoy, K., Sethumadhavan, S., Woo, H.K., Jang, H.G., Jha, A.K., *et al.* (2011). Functional genomics reveal that the serine synthesis pathway is essential in breast cancer. Nature *476*, 346-350.

Trapnell, C., Williams, B.A., Pertea, G., Mortazavi, A., Kwan, G., van Baren, M.J., Salzberg, S.L., Wold, B.J., and Pachter, L. (2010). Transcript assembly and quantification by RNA-Seq reveals unannotated transcripts and isoform switching during cell differentiation. Nature biotechnology *28*, 511-515.

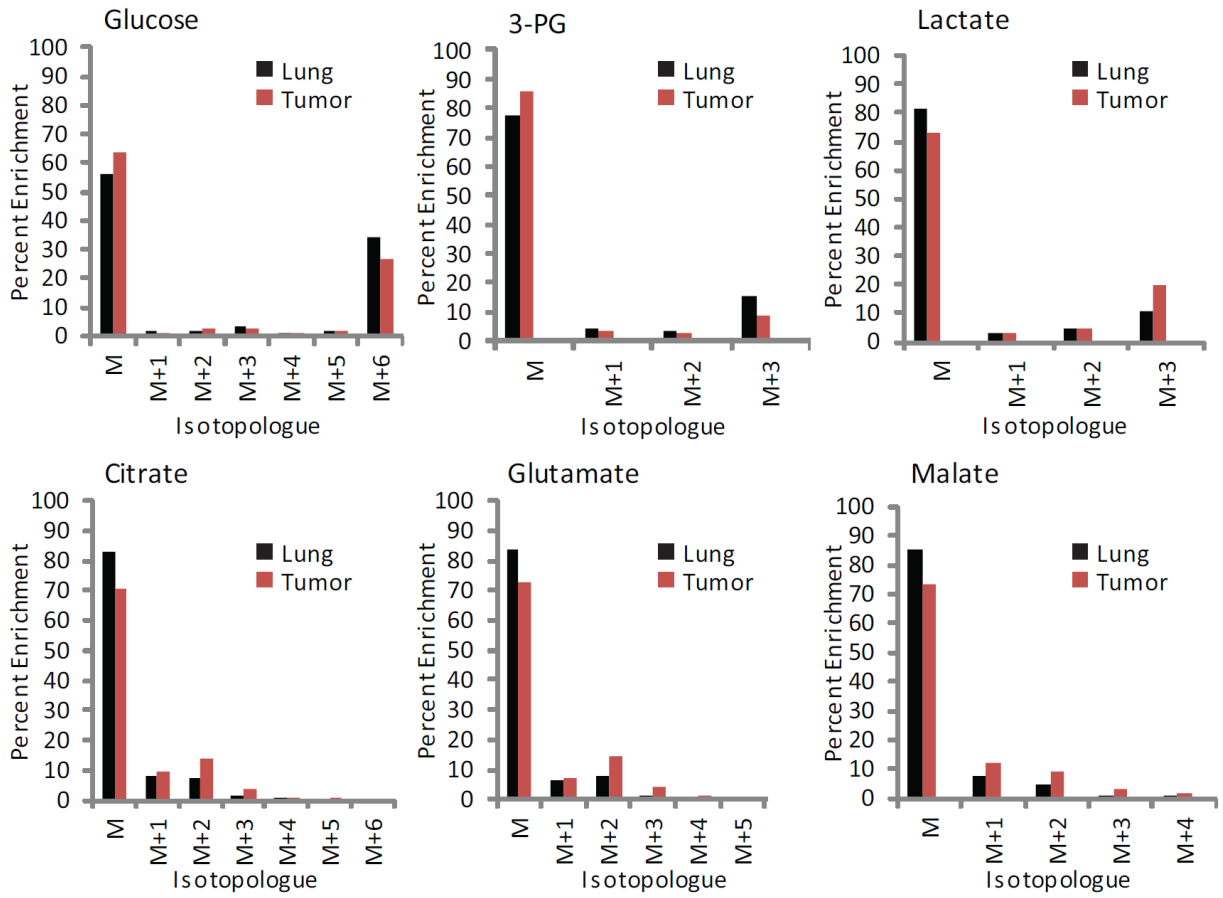


**Figure S1. Complete isotopologue distributions for metabolites in Figure 1E.** Related to Figure 1. Enrichments in tumor and in adjacent lung tissue are shown for each metabolite.

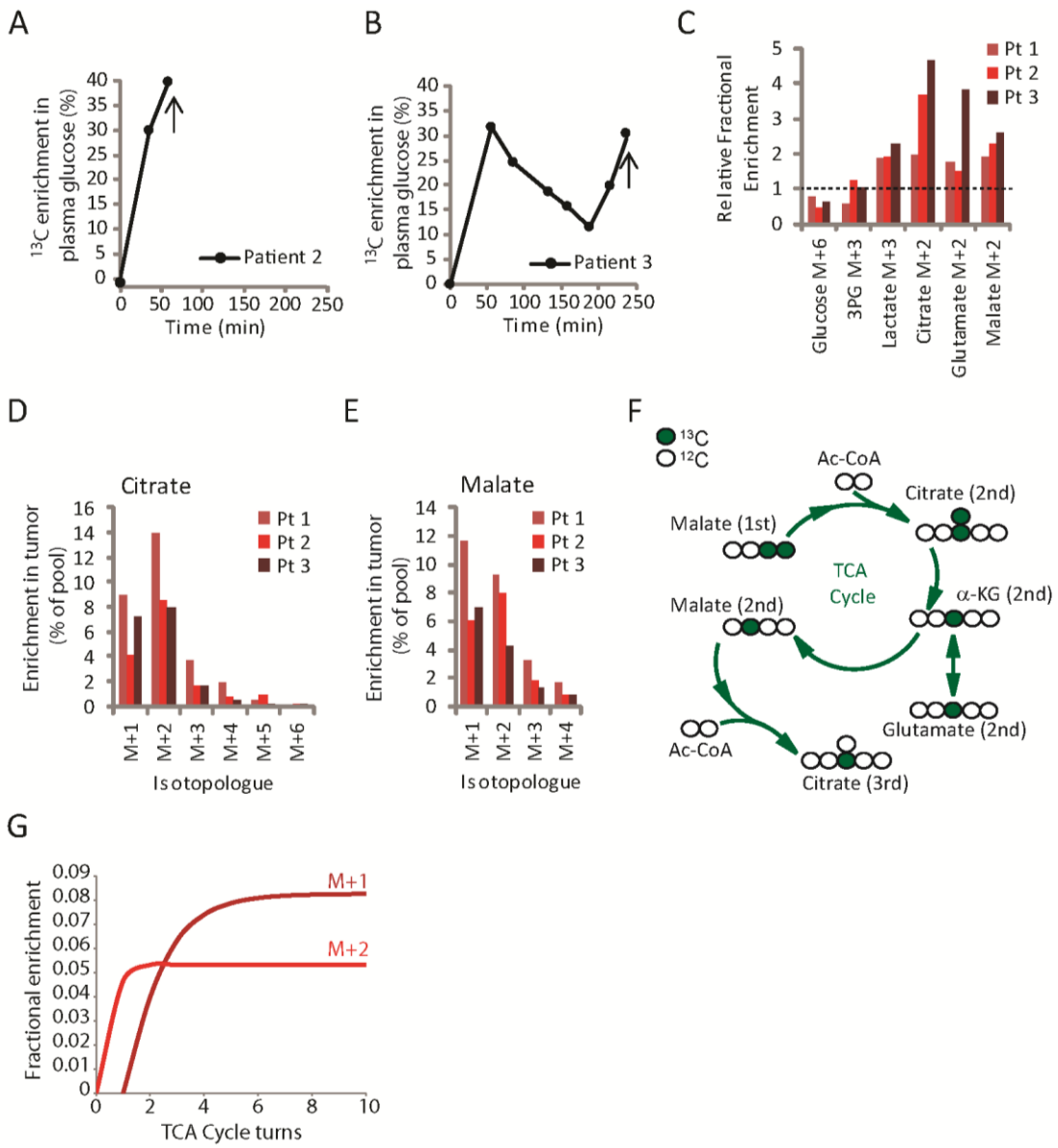


**Figure S2. Comparison between bolus and continuous infusions of [U-$^{13}$C]glucose.** Related to Figure 2.

(A-B) Plasma glucose enrichment after [U-$^{13}$C]glucose boluses in patients 2 and 3. Arrows indicate tumor removal.

(C) Relative enrichment (tumor/lung) of glucose and several glucose-derived metabolites in patients 1-3. Patient 1's data is also displayed in Fig. 1E and is shown here for comparison to patients 2 and 3.

(D) Mass isotopologue distribution of tumor citrate in patients 1, 2, and 3.

(E) Mass isotopologue distribution of tumor malate in patients 1, 2, and 3.

(F) Likely origin of M+1 isotopologues during [U-$^{13}$C] glucose administration. The pathway begins with the malate M+2 arising in the first turn of the TCA cycle, after condensation of acetyl-CoA M+2 with unlabeled OAA. Because the enrichment of acetyl-CoA is low, subsequent turns of the cycle are much more likely to incorporate unlabeled rather than labeled acetyl-CoA.

(G) Relationship between M+1 and M+2 in malate from [U-$^{13}$C]glucose, as simulated by tcaSIM during progressive turns of the TCA cycle. This simulation used average tumor fractional enrichments for 3-PG (0.11) and average values for PDH and PC flux (0.47 and 0.11, respectively). Other anaplerotic fluxes were set to 0.

*Abbreviations*: Ac-CoA, acetyl-Coenzyme A; α-KG, α-ketoglutarate.

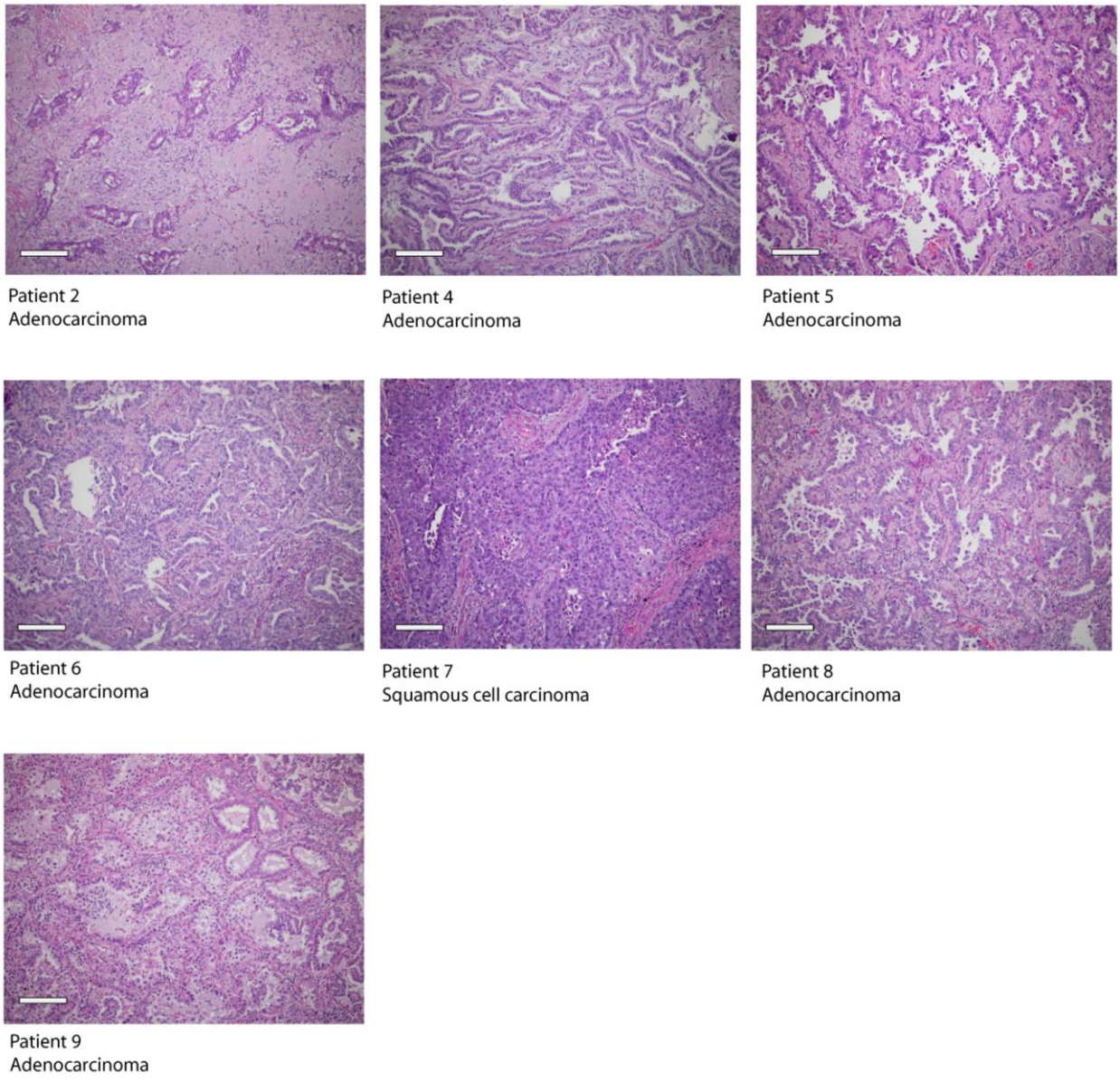


**Figure S3. Sample hematoxylin/eosin-stained histopathology samples.** Related to Figure 2. Samples from Patient 1 are in Figure 1. Patient 3 had no tissue available for additional analysis. Other details about all 9 tumors are in Table 1. Scale bar 200μm.

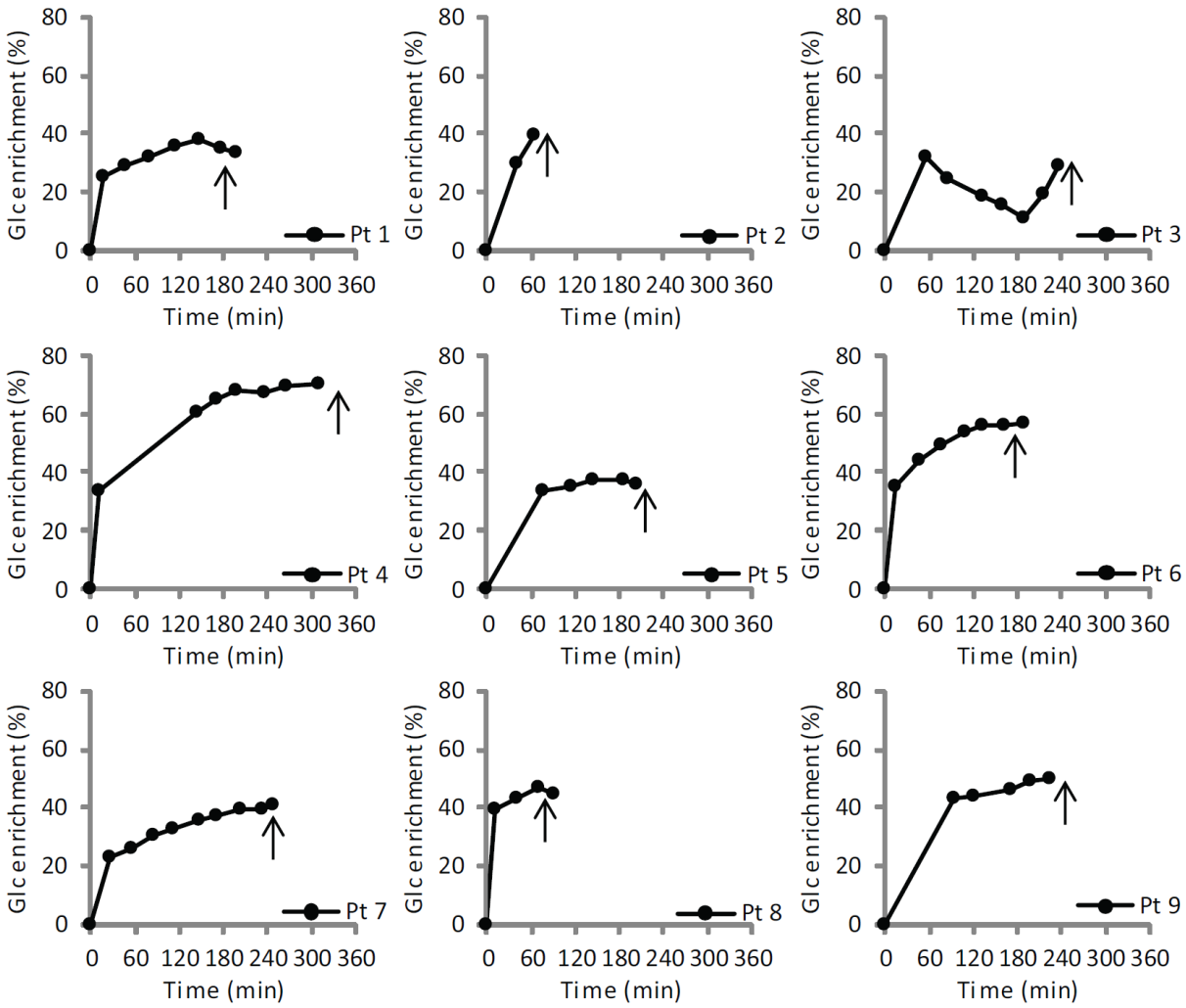


**Figure S4. $^{13}$C plasma glucose enrichment curves for all patients in the study.** Related to Figure 2. In most patients, a bolus of [U-$^{13}$C]glucose was administered over a ten minute period, followed by continuous infusion of [U-$^{13}$C]glucose until resection of the affected lobe. Patients 2 and 3 received boluses of [U-$^{13}$C]glucose as explained in the text. Arrows indicate the time of tumor resection, either right before or immediately after the last blood draw. Abbreviations: Glc, Glucose; Pt, Patient; min, minutes.

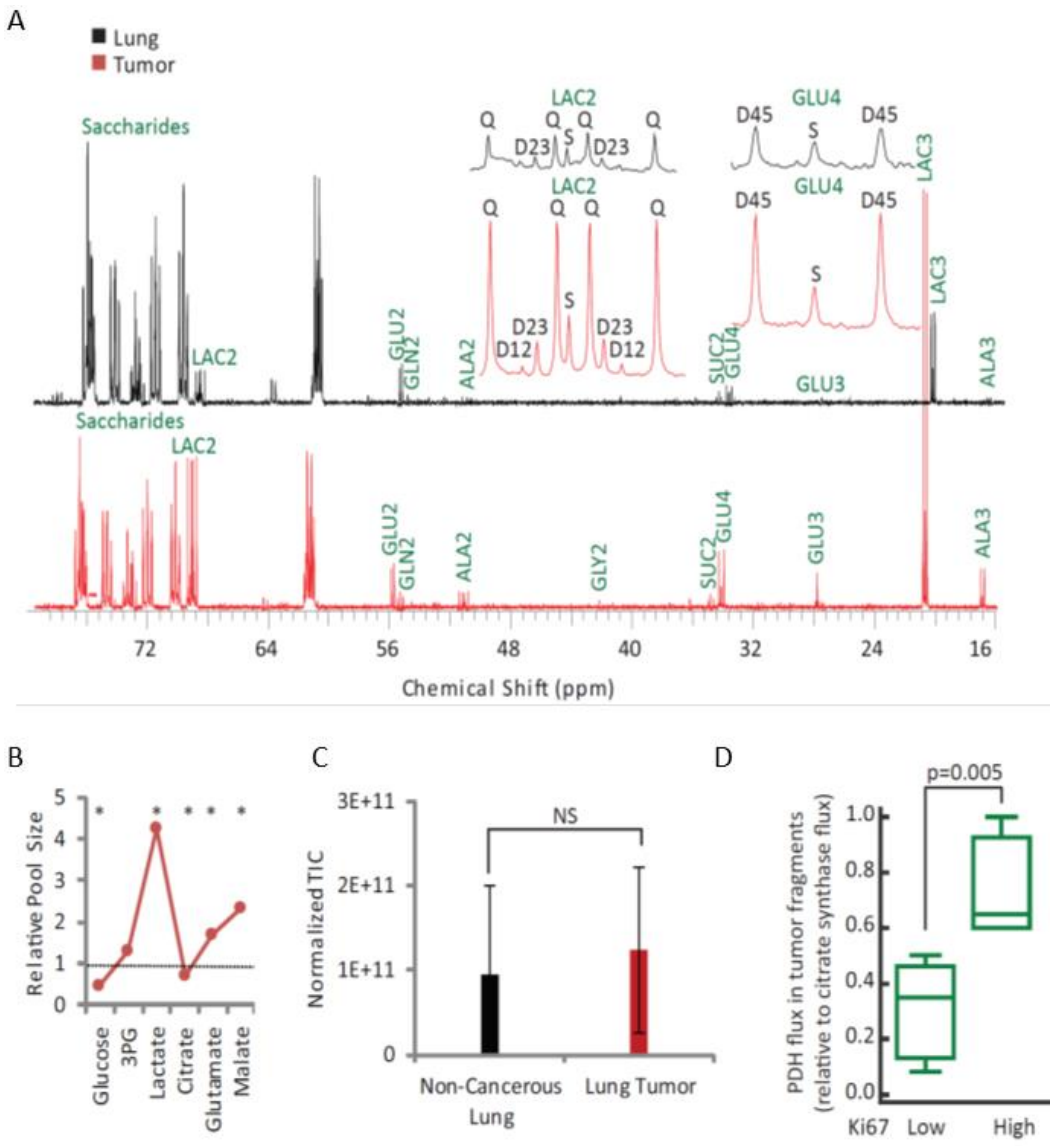


**Figure S5. NMR spectroscopy, metabolite abundance, and PDH activities in human NSCLC samples.** Related to Figure 3.

(A) These spectra are from patient 5. Abbreviations are explained in Figure 3A.
(B) Average abundance of metabolites analyzed for $^{13}C$ enrichment. Abundance is expressed as tumor/lung, with the abundance in the lung normalized to 1.0 (dashed line). *, $p < 0.05$ by paired Student's t-test.
(C) Analysis of total metabolite abundance in lung and tumor samples. Normalized total ion current (TIC) is the product of TIC and mg of protein from each fragment. Data are the average and S.D. of all fragments. NS, not significant by paired Student's t-test.
(D) Apparent PDH fluxes in regions with both $^{13}C$ labeling data and quantitation of Ki67-positive tumor cells. "Low" Ki67 fragments are those in which the fraction of cells with Ki67-positive nuclei is under 25%. "High" fragments are those in which 25% or more tumor cells have Ki67-positive nuclei.

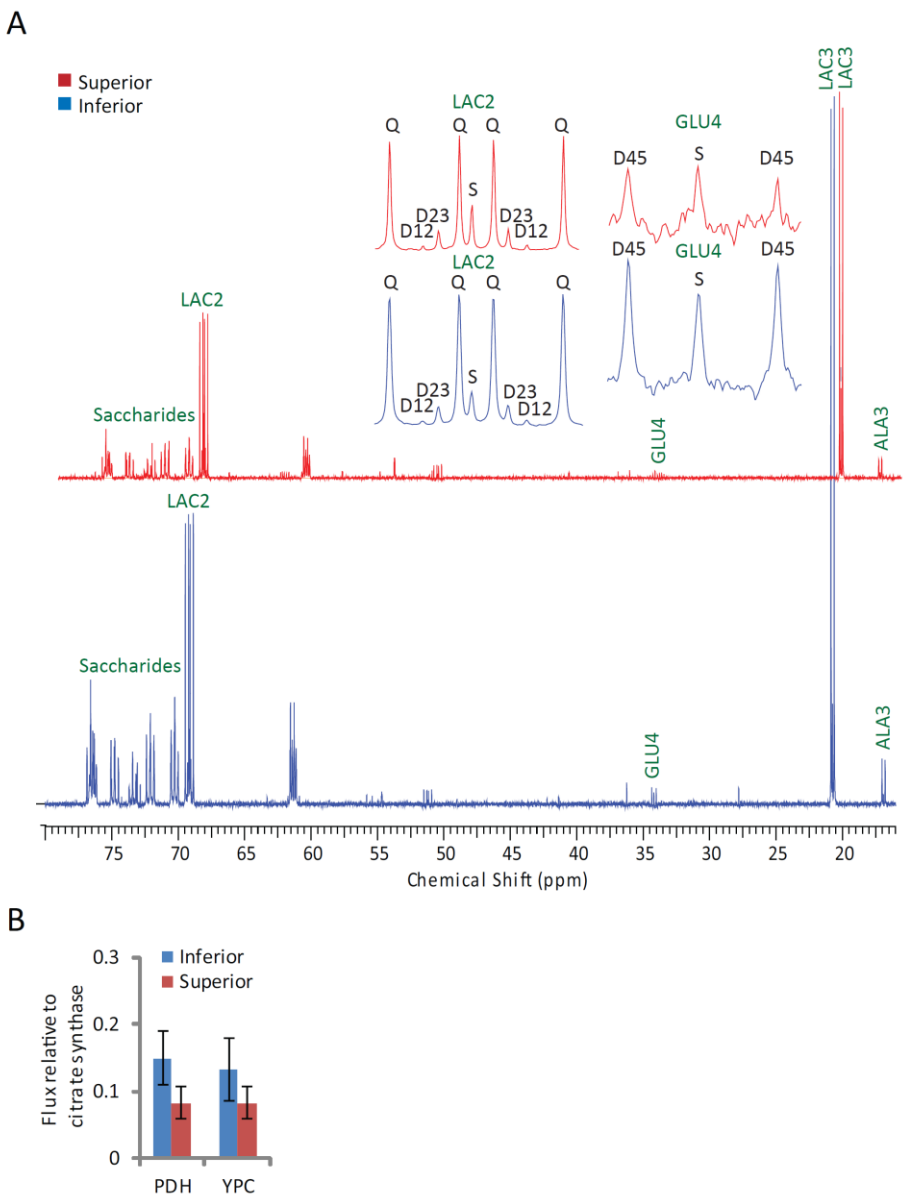


**Figure S6. Metabolic heterogeneity within a single, well-perfused NSCLC tumor from Patient 8.** Related to Figure 5.

(A) $^{13}$C NMR spectra from fragments taken from the superior and inferior regions (higher and lower DCE, respectively) of patient 8's adenocarcinoma. GC/MS analysis of these tissue samples is shown in Figure 5F.
(B) tcaSIM modeling of $^{13}$C data from three fragments from each of the two regions. Data are the average and S.D. of individual flux estimations.

*Abbreviations:* ppm, parts per million; S, singlet; D, doublet; Q, quartet; LAC, Lactate; GLU, Glutamate; ALA, Alanine; PDH, Pyruvate Dehydrogenase; YPC, Pyruvate Carboxylase.

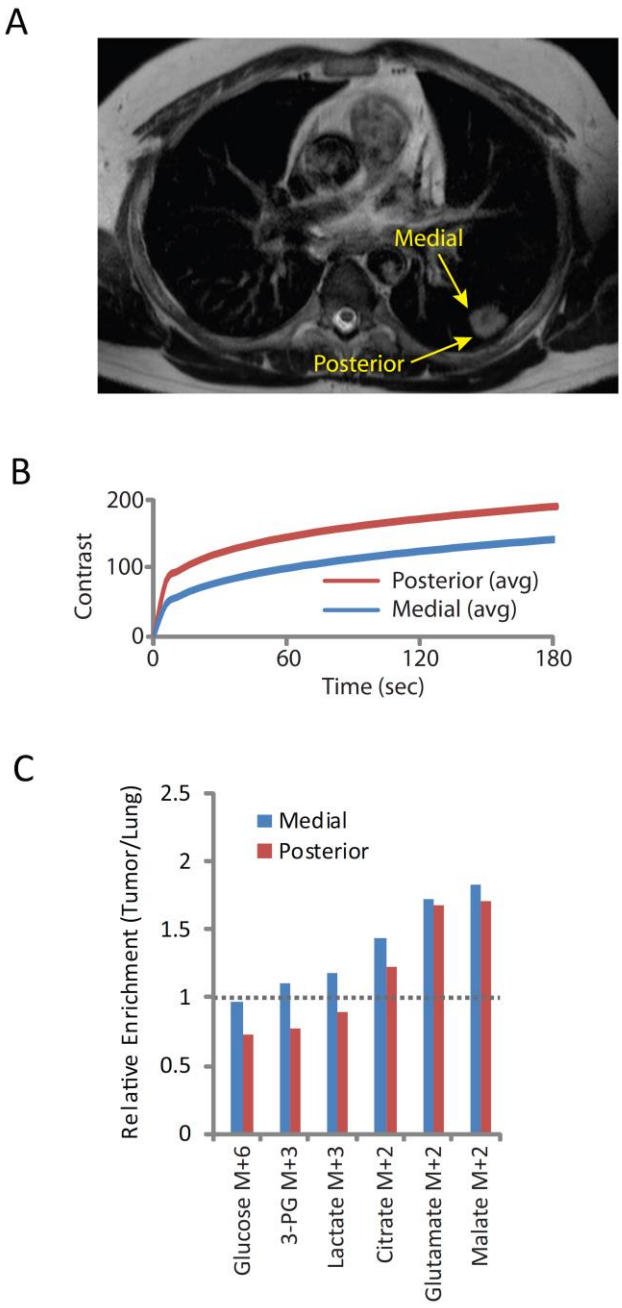


**Figure S7. Metabolic heterogeneity within a single, less-perfused NSCLC tumor from Patient 9.** Related to Figure 5.

(A) MRI of patient 9's adenocarcinoma. DCE was analyzed in the medial and posterior aspects of the tumor.
(B) DCE curves from posterior and medial regions, demonstrating somewhat higher DCE signal in the posterior region.
(C) Relative $^{13}C$ enrichment in samples taken from the medial and posterior aspects of the tumor. Enrichments are expressed as the tumor/lung ratio, with enrichment in the lung normalized to 1.0 (dashed line).